Available online at www.sciencedirect.com
SCIENCE DIRECT®
Journal of Power Sources 130 (2004) 192–201
JOURNAL OF POWER SOURCES
www.elsevier.com/locate/jpowsour

Fuel economy of hydrogen fuel cell vehicles

Rajesh K. Ahluwalia*, X. Wang, A. Rousseau, R. Kumar
Argonne National Laboratory, 9700 South Cass Avenue, Argonne, IL 60439, USA

Received 28 November 2003; accepted 15 December 2003

Abstract

On the basis of on-road energy consumption, fuel economy (FE) of hydrogen fuel cell light-duty vehicles is projected to be 2.5–2.7 times the fuel economy of the conventional gasoline internal combustion engine vehicles (ICEV) on the same platforms. Even with a less efficient but higher power density 0.6 V per cell than the base case 0.7 V per cell at the rated power point, the hydrogen fuel cell vehicles are projected to offer essentially the same fuel economy multiplier. The key to obtaining high fuel economy as measured on standardized urban and highway drive schedules lies in maintaining high efficiency of the fuel cell (FC) system at low loads. To achieve this, besides a high performance fuel cell stack, low parasitic losses in the air management system (i.e., turndown and part load efficiencies of the compressor–expander module) are critical.

Keywords: Fuel economy; Hydrogen fuel cell; Light-duty vehicles

1. Introduction

Almost all of the major automobile manufacturers around the world are actively engaged in developing prototype fuel cell (FC) vehicles to meet the future transportation needs of people in developed and developing countries. Hydrogen-fueled fuel cell vehicles (H_2-FCVs) are also an essential component of the hydrogen economy—a vision of clean, sustainable energy for future generations. For developed countries, such fuel cell vehicles hold the promise of greatly reduced urban pollution and decreased dependence on imported petroleum. For developing countries, H_2-FCVs also offer an attractive alternative to vastly increasing their petroleum imports, refining, and distribution infrastructure. Underlying these projected benefits is the higher efficiency of fuel cell systems compared to conventional gasoline-fueled internal combustion engines (ICEs). In this paper, we present and discuss the results of an analytical study to examine the potential for fuel economy gains by fuel cell vehicles over the conventional gasoline-fueled passenger cars. Such analyses also help to determine the amounts of hydrogen such vehicles will need to carry onboard to achieve the desired driving range between refuelings.

We quantify the potential gain in fuel economy (FE) in terms of a multiplier which is defined as the ratio of the miles per gallon gasoline equivalent (mpgge) achieved by the hydrogen fuel cell vehicle on standardized drive schedules to the miles per gallon gasoline achieved by the reference gasoline internal combustion engine vehicle (ICEV) on the same drive cycles. In calculating the multiplier, hydrogen is converted to an equivalent amount of gasoline that has the same lower heating value. According to this conversion, one kg of hydrogen is approximately equivalent to one US gallon of gasoline in heating value.

Several well-to-wheel studies have also evaluated the fuel economy of H_2-FCVs relative to their conventional gasoline ICEV counterparts. Two of these studies are particularly noteworthy because of the extremes in the methodologies employed. The MIT study [1] broadly defines the performance of the fuel cell system by a simple tabulation of the integrated efficiency as a function of the fraction of peak power and makes gross assumptions for the specific power of the FC propulsion system. Other components of the propulsion system and the vehicle power demand were simulated in much greater detail. For a typical US mid-size family sedan, the MIT study estimated the fuel economy of future H_2-FCVs to be 3.5–3.8 times that of the reference 2001 gasoline ICEV. The future H_2-FCV platform in this study was lighter, more aerodynamic, and had lower rolling resistance coefficient and a smaller frontal area than the reference ICEV. With the ICE and fuel cell systems on the same

* Corresponding author. Tel.: +1-630-252-5979; fax: +1-630-252-5287.
E-mail address: walia@anl.gov (R.K. Ahluwalia).

0378-7753/$ – see front matter © 2004 Elsevier B.V. All rights reserved.
doi:10.1016/j.jpowsour.2003.12.061

vehicle platforms and with projected advancements in the internal combustion engine technology, the study estimated the fuel economy of the future FC vehicle to be 2.2–2.4 times the fuel economy of the future (2020) gasoline ICE vehicle.

The GM study [2] modeled the complete vehicle architecture and designed the components to meet specified performance requirements such as 0–60 mph acceleration time, passing maneuvers, top speed and gradeability. The baseline vehicle selected for this study was the Chevrolet Silverado full-size pickup truck. Details of the FC system are considered proprietary but the performance was stated to be a projection of experimental data obtained in GM's laboratories. The study conducted a statistical analysis to provide a best estimate and a measure of the uncertainty around the best estimate. At the 50% likelihood point, the GM study estimated the fuel economy of the H_2-FCVs to be 2.1 times that of the ICEV for year 2005 and beyond.

2. Fuel cell system

Pressurized and ambient pressure polymer electrolyte fuel cell (PEFC) systems are being developed for automotive propulsion and other applications. Pressurization permits fuel cell operation at a higher temperature (e.g., 80 °C for 3 atm versus 60–70 °C for 1 atm), which eases thermal management, improves cell performance thereby decreasing the required cell active area (hence, volume, weight, and cost), and facilitates water recovery. The scope of the present study is limited to pressurized hydrogen-fueled automotive PEFC systems of the type shown schematically in Fig. 1.

It is assumed in this study that the FC system operates at 2.5 atm (absolute) at the rated power point; the operating pressure decreases at partial loads according to the performance map of the compressor–expander module (CEM). At the rated power point, the average cell voltage is 0.7 V, and the nominal operating temperature of the fuel cell stack is 80 °C. At part load, the cell voltage is higher than 0.7 V and it may not be possible to maintain the stack at 80 °C. The hydrogen and the air fed to the fuel cell stack are humidified to a relative humidity of 90% at the stack's operating temperature.

The fuel cell power system shown in Fig. 1 may be described in terms of three circuits—one each for the hydrogen, air, and process water. In addition, a coolant circuit is used for thermal management in the system.

Hydrogen from the source (e.g., a compressed gas cylinder) is humidified by using process water and heat from the coolant circuit. The humidified hydrogen is fed to the fuel cell stack; the excess is recirculated to avoid any stagnant zones.

Ambient air is compressed, humidified, and fed to the fuel cell stack at a rate nominally twice that needed for the electrochemical oxidation of the hydrogen to achieve 50% oxygen utilization. During deceleration and at low loads, it may not be feasible to rapidly decrease the air flow rate to achieve 50% oxygen utilization. Exhaust air from the fuel cell stack is cooled in a condenser to recover process water, and then expanded through the turbine to provide some of the compression energy.

Process water is pumped from the tank to the hydrogen and air humidifiers. Inertial separators at the exits from the stack, condenser, and expander recover water from the air stream and return it to the process water tank.

The coolant, which may be water or other fluid, removes waste heat from the fuel cell stack and provides the heat to vaporize water at the gas humidifiers. Excess waste heat is rejected to the ambient air at the radiator–condenser. Al-

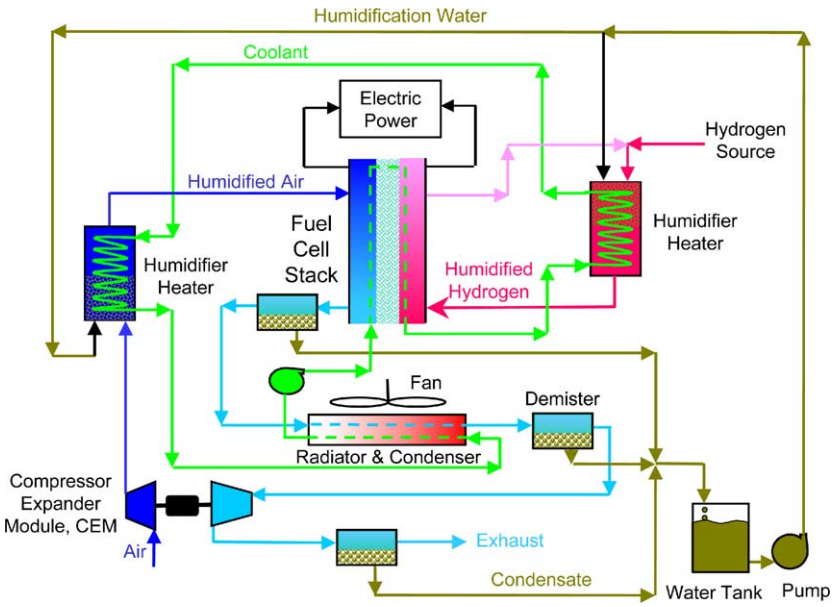

Fig. 1. Schematic diagram of a hydrogen-fueled, polymer electrolyte fuel cell system for automotive applications.

though not shown in Fig. 1, the coolant circuit can also provide heat to the passenger cabin, as is done in today's vehicles.

Alternative fuel cell system configurations may also be considered, but they are not discussed in this paper.

3. Performance of fuel cell system

The performance of the hydrogen fuel cell system shown in Fig. 1 was analyzed with GCtool [3], a systems design and analysis software package developed at Argonne National Laboratory. Although the comprehensive analysis considers heat, mass and energy flows into and out of each component, only the aspects pertaining to energy efficiency are discussed below.

3.1. Air management system

Developers are pursuing different options for delivery of compressed air to the cathode side of the fuel cell stack. These include a twin-screw compressor, centrifugal compressor and expander on a common shaft, and a toroidal intersecting vane machine [4]. Results presented in this work are based on the projected performance shown in Fig. 2 for a turbo compressor–expander module being developed by Honeywell [5]. This module uses a mixed axial and radial flow compressor matched to, and on a common shaft with, an expander with variable inlet nozzle vanes. Because of relatively small flow, less than 200 g/s for a 160 kW FC system, the shaft spins at speeds exceeding 90,000 rpm at the design point. The shaft is supported on air bearings that require a minimum speed of about 36,000 rpm to maintain the air cushion. The module is equipped with a high-speed AC induction motor and a motor controller that also includes a DC/AC inverter so that the module can be directly run by the DC power generated by the PEFC stack. Over the operating range, the motor has an efficiency of about 91% and the motor-controller has an efficiency of about 92%. At the design point, the compressor delivers air at 2.5 atm and the compressor and expander have isentropic efficiencies of about 80 and 78%, respectively. With a 20.4 kPa (~3 psi) pressure drop between the compressor and expander, i.e., across the air heater–humidifier, PEFC stack and the condenser, the module for a 160 kW FC system requires a mechanical power of 7.7 kW at the shaft and a DC power input of 9.1 kW to the motor controller. At part load, the isentropic efficiency of the compressor decreases only gradually from 80% at design point to 72% at one-fourth of the rated flow; the efficiency drops off rapidly as the flow is further reduced towards idling conditions. The expander efficiency behaves similarly. Even though the compressor and expander efficiencies decrease at part load, the net power consumed by the CEM per unit of air flow is actually lower than at rated power because of the drop-off in the compressor discharge pressure.

3.2. PEFC stack

Fig. 3 shows the polarization curves used in this study. The curves are based on a correlation of cell voltage as a function of current density, temperature and oxygen partial pressure. The experimental data underlying the correlation may be somewhat dated but show the proper trend with respect to the independent variables. Consistent with the reported performances of GM2001 [6] and Ballard stacks [7], PEFC system weights and volumes were estimated by using the published stack power density and specific weight and adjusting them for the design-point cell voltage. For example, the GM2001 stack with 640 cells was stated to

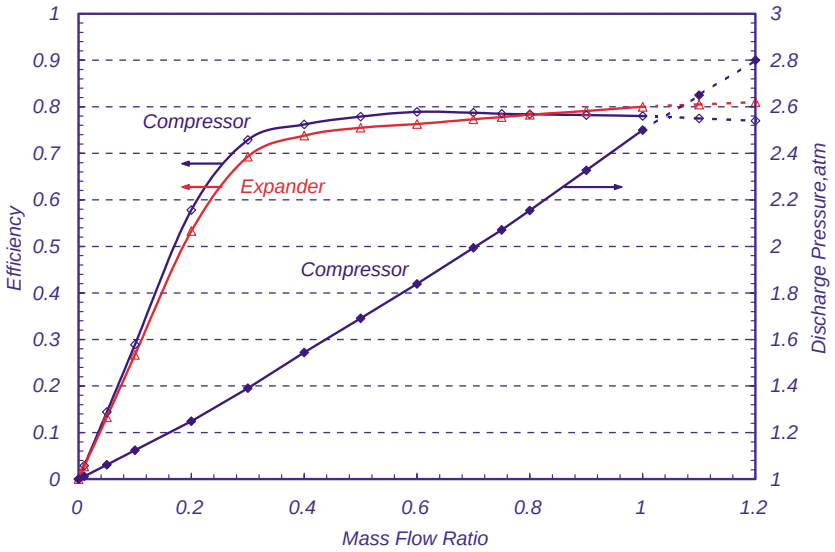

Fig. 2. CEM performance map: isentropic efficiencies of turbo-compressor–expander and compressor discharge pressure.

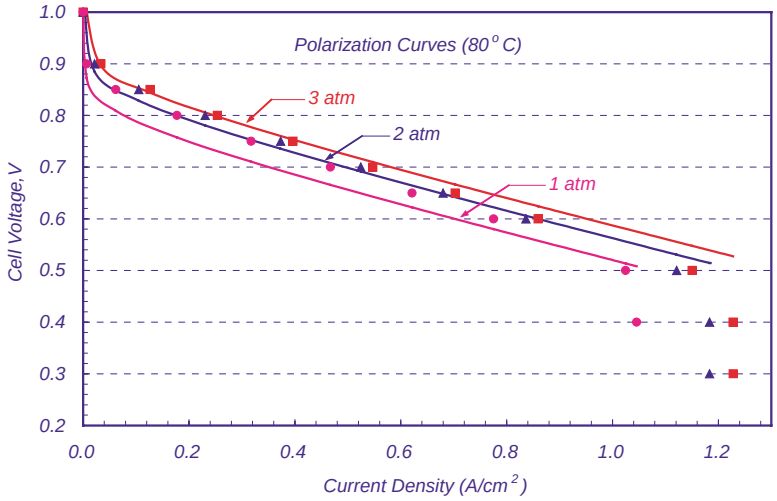

Fig. 3. Polarization curves at 80 °C determined from a correlation (solid lines) and a model constructed from laboratory data taken on a small cell (symbols).

have a power density of 1.75 kW/l and specific power of 1.25 kW/kg. Within the simulation model, the current density abscissa in Fig. 3 is renormalized to match the assumed power density at the design point.

3.3. PEFC system performance

Table 1 shows the steady-state performance attributes of three representative stand-alone fuel cell systems. The air management system for FCS-1 includes both a compressor and an expander and the design-point cell voltage is 0.7 V. It has an overall efficiency of 50.6% (based on the lower heating value of hydrogen) at rated power and 61.6% at 25% of rated power.

FCS-2 is similar to FCS-1 except that it does not have an expander. As a result, the compressor in FCS-2 requires an electric motor that is nearly three times the rated capacity of the motor in FCS-1. The FCS-2 has an overall efficiency of 47.0% at rated power and 61.5% at quarter power.

FCS-3 differs from FCS-1 in that the cell voltage at rated power is 0.6 V. FCS-3 has on overall efficiency of only 43.2% at rated power and 60.1% at quarter power.

Table 1
Attributes of scalable 160 kW fuel cell systems

	FCS-1	FCS-2	FCS-3
Air management system	With expander	Without expander	With expander
Design point cell voltage (V)	0.7	0.7	0.6
CEM motor power (kW)	7.7	22.3	9.0
FCS efficiency			
Rated power (%)	50.6	47.0	43.2
50% power (%)	58.3	57.5	55.5
25% power (%)	61.6	61.5	60.1
Specific power (W/kg)	360	320	400

Also included in Table 1 are the specific powers of the three fuel cell systems. The specific power of FCS-2 is about 10% lower than that of FCS-1 primarily because the stack has to generate additional power to compensate for the power produced by the expander in FCS-1. Because of lower efficiency, the balance of plant is also somewhat larger. The specific power of FCS-3 is about 10% higher than that of FCS-1. The stack for FCS-3 has higher power density because it is sized for a lower cell voltage, but the balance-of-plant is larger due to the lower overall system efficiency at rated power.

The maximum allowable turndown of the CEM is also an important parameter that affects the system efficiency at part load as well as oxygen utilization and water balance. This limiting turndown is determined by the minimum idle speed defined as the shaft rpm at which the air management system can provide sufficient cathode air to enable the FCS to generate the power needed by the CEM. This definition is appropriate for a stand-alone FCS in which all FCS accessory loads are provided by the stack. In general, the idle speed may be determined by the power input to the motor controller and by the design of the CEM. For example, in the Honeywell design the air bearings require a minimum speed of 36,000 rpm to support the shaft. Our simulations for the high-speed CEM indicate that with an expander in the system, the idle speed can be as low as 42,500 rpm and the corresponding maximum turndown as high as 20. Without an expander, the minimum idle speed may be as high as 51,500 rpm corresponding to a maximum turndown as low as five.

Fig. 4 illustrates the effect of CEM turndown on dynamic efficiency of FCS-1, the system with an expander, along a simulated urban drive cycle. Simulation results are presented for two variations of FCS-1, one with the theoretically-achievable maximum turndown of 20 and the other with a maximum turndown of five. Differences in efficiencies for the two simulations are clearly evident at low

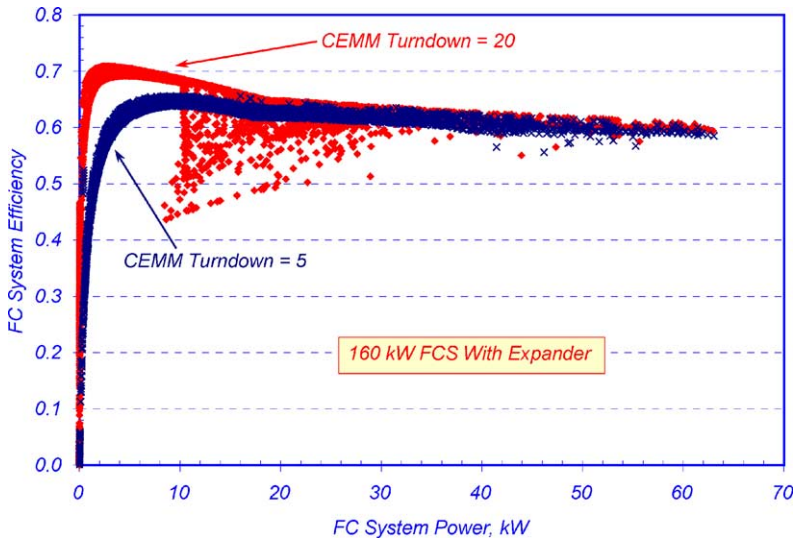

Fig. 4. Effect of CEM turndown on dynamic system efficiency for an urban drive cycle.

loads. Whereas both give efficiencies in excess of 60% on the urban drive cycle the peak efficiency can be greater than 70% at low loads for the system with a maximum turndown of 20. However the scatter in efficiency is also wider at maximum turndown of 20. This scatter is largely due to acceleration demands that are made with the shaft rpm near the idle speed. At these instances, the CEM motor–controller draws large power from PEFC stack to ramp up the shaft speed and increase the cathode flow to meet the surge in demand. The power consumed by the motor is a parasitic loss and contributes to lowering of dynamic efficiency. The frequency and magnitude of the shaft acceleration events are greater at 42,500 rpm idle speed (maximum turndown of 20) than at 51,500 rpm idle speed (maximum turndown of five). During the acceleration events, the dynamic system efficiency is lower than the steady-state efficiency. Conversely, the dynamic efficiency can be greater than the steady-state efficiency during the deceleration events because some of the CEM parasitic power can be supplied by the inertial power stored in the shaft, compressor, expander and motor.

For an urban drive cycle, Fig. 5 compares the dynamic efficiencies of FCS-1, the system with an expander, and FCS-2, the system without an expander. In these simulations, FCS-1 is assumed to have the maximum turndown achievable with an expander (20) and FCS-2 the maximum turndown achievable without an expander (five). The differences in efficiencies at high loads are due to the additional power generated by the expander in FCS-1. At low loads, where the parasitic power consumed by the CEM as a fraction of the power produced by the FCS is small, the differences in efficiencies are due to the larger turndown available with the expander in FCS-1. FCS-1 shows a wide scatter in dynamic

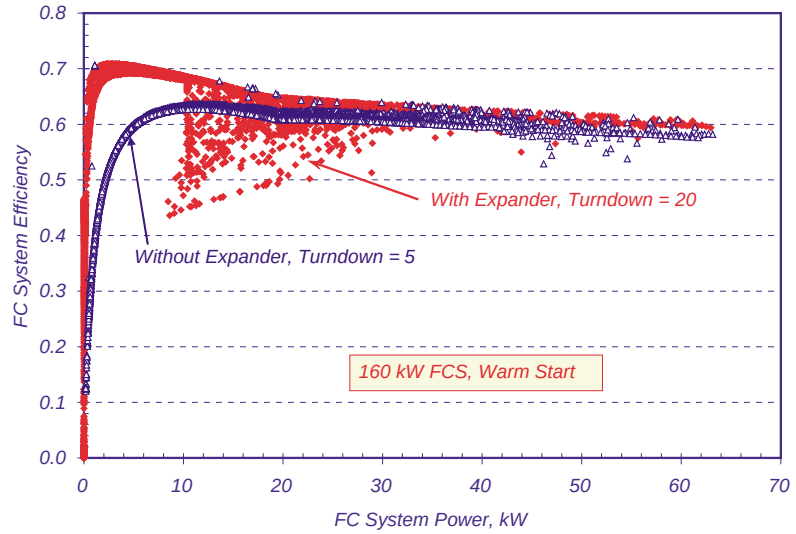

Fig. 5. Effect of expander on dynamic system efficiency for an urban drive cycle.

efficiency at low loads (10–30 kW) whereas FCS-2 exhibits only minor fluctuations. At higher loads (35–60 kW), efficiency fluctuations are damped in FCS-1 but amplified in FCS-2. In general, efficiency fluctuations appear in a narrow band of power demand starting at P/N where P is the rated power and N is the CEM turndown. More importantly, for power demand less than P/N, the oxygen utilization is much lower than the design value of 50% and water recovery becomes an issue.

4. Performance of fuel cell vehicles

The performance of the hydrogen fuel cell vehicles was modeled by integrating GCtool with the PSAT vehicle simulation software [8], also developed at Argonne. For this study, we analyzed three US vehicle platforms: the compact Chevrolet Cavalier, the mid-size Ford Taurus, and the sport utility vehicle (SUV) Ford Explorer. We simulated the performance of each vehicle with a gasoline ICE and a hydrogen fuel cell (H_2-FC) power plant. Each vehicle was simulated over the US Federal Urban Driving Schedule (FUDS) (Fig. 6) and the Federal Highway Driving Schedule (FHDS) (Fig. 7). We then determined the FUDS, FHDS, and combined (a weighted harmonic mean of the two) fuel economies for each vehicle/power train combination.

Table 2 provides values for the major vehicle parameters that affect the fuel economy, including mass, drag coefficient, frontal area, and coefficient of rolling friction. The values for the hydrogen platform are based on FCS-1, the fuel cell system with an expander and PEFC stack at a design-point cell voltage of 0.7 V. For each vehicle, the test

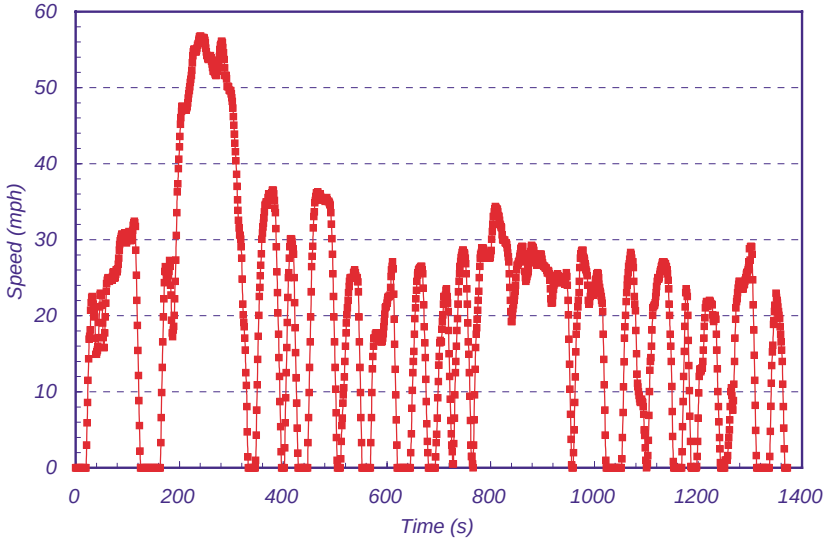

Fig. 6. Vehicle speed vs. time for the Federal Urban Driving Schedule.

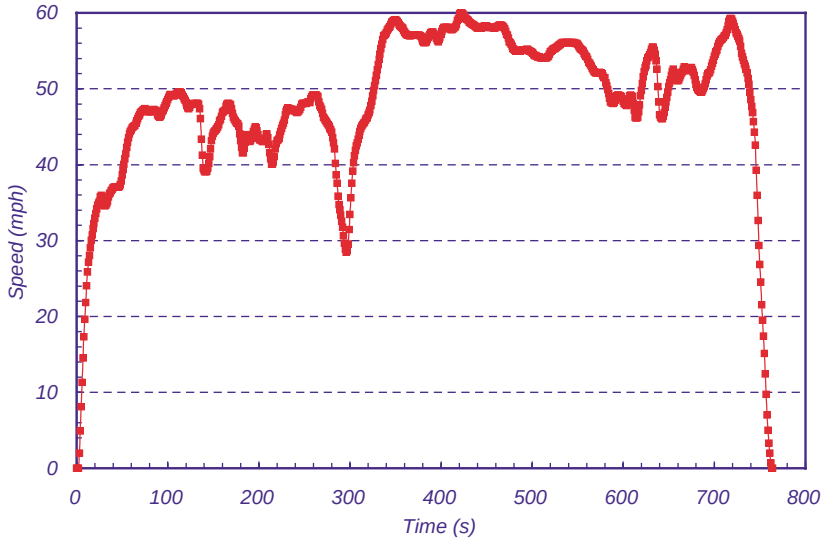

Fig. 7. Vehicle speed vs. time for the Federal Highway Driving Schedule.

Table 2
Values of key vehicle simulation parameters used in the analyses

Parameter	Cavalier		Taurus		Explorer	
	ICE	H_2-FC	ICE	H_2-FC	ICE	H_2-FC
Mass (kg)	1.214	1.400	1.693	1.850	2.055	2.320
Drag coefficient	0.38		0.32		0.41	
Frontal area (m^2)	1.8		2.2		2.46	
Coefficient of rolling friction	0.009		0.009		0.0084	
Engine power (kW)	86	90	116	120	160	160

mass of the hydrogen version is greater than that of the gasoline version to account for the lower fuel storage energy density and fuel cell system power density. Table 2 also shows the gasoline engine power (mechanical) and the net fuel cell system power (electrical) needed to provide similar drivability characteristics for the fuel cell version of the vehicle. Other vehicle parameters are the same for the two versions of each vehicle.

The modeled electric drivetrain for the FC vehicles consists of a permanent magnet AC traction motor followed by a one-speed transmission and a final drive. The efficiency and torque map of the traction motor includes a DC/AC inverter that is scaled from the data obtained in our laboratory. The electric motor–inverter has a combined peak efficiency of 94%. The one-speed transmission is assigned a constant efficiency of 97% and the final drive a constant efficiency of 93%. It is assumed that the traction motor–inverter is directly connected to the PEFC stack without an intermediate DC/DC converter.

4.1. Fuel economy

Table 3 lists the fuel economy results from base case simulations (i.e., using the FCS-1 fuel cell system configuration) of the six vehicle cases discussed above. The table shows the miles per gallon of gasoline (mpg) or gasoline equivalent (mpgge, based on the lower heating value (LHV) of the fuel) for the different vehicles, power trains, and driving schedules. The US Environmental Protection Agency (EPA) fuel economy ratings for the three conventional gasoline-fueled vehicles are also listed in Table 3 for comparison. In general, there is good agreement between the simulated combined cycle mpg and the values obtained by EPA for the conventional vehicles. The small differences arise from factors such as the engine performance maps in PSAT not being identical to the actual engine performance in the vehicles tested by EPA. The listed fuel economies have separate correction factors for FUDS and FHDS applied to the calculated values to reflect real-world driving experiences. EPA applies the same correction factors to the fuel economies of conventional vehicles measured on test tracks; we have assumed that they are applicable to FC vehicles as well.

Table 3 also shows the fuel economy multiplier for the H_2-FCVs versus the ICEVs for the combined urban and highway driving simulations. The multiplier is 2.7 for the compact Cavalier and mid-size Taurus and 2.5 for the SUV. For all three vehicle platforms the multiplier is higher over FUDS (e.g., 2.6 for SUV) than over FHDS (e.g., 2.3 for SUV). The FHDS to FUDS (FUDS has a lower average speed and power demand than FHDS.) mpgge ratio is higher for ICEVs (e.g., 1.3 for SUV) than for the H_2-FCVs (e.g., 1.1 for SUV). This result simply reinforces our understanding that whereas the efficiency of an ICE decreases at part load that of the H_2 FCS generally increases at part load.

We also examined the sensitivity of these results to variations in several fuel cell and vehicle design and operating parameters. For the fuel cell system, these included the fuel cell polarization curves, the design point cell voltage, and the configuration of and the parasitic losses in the CEM. Vehicle parameters investigated included vehicle mass, drag coefficient, and the coefficient of rolling friction.

4.2. Effects of fuel cell system parameters

The base case analyses discussed above employed reference cell polarization curves based on a published cor-

Table 3
Calculated fuel economies of conventional (ICE) and fuel cell (H_2-FC) vehicles

Parameter		Cavalier		Taurus		Explorer	
		ICE	H_2-FC	ICE	H_2-FC	ICE	H_2-FC
Fuel economy (mpgge)	FUDS	25	73	20	58	18	47
	FHDS	32	75	29	69	23	54
	Combined	27.6	73.8	23.2	62.4	19.8	49.7
H_2-FC/ICE (mpgge)		2.7		2.7		2.5	
EPA fuel economy combined (mpgge)		26.0		23.7		18.4	

Table 4
Effect of fuel cell system parameters on fuel economy of SUV

FCS configuration	Cell voltage at rated power (V)	CEM maximum turndown	FUDS (mpgge)	FHDS (mpgge)	Combined (mpgge)	FC/ICE (mpgge)	Change in FE (%)
Base case							
FCS-1	0.7	20	46.1	53.0	49.0	2.5	0
More aggressive polarization curve							
FCS-1	0.7	20	49.0	56.1	52.0	2.6	6.1
Effect of cell voltage at rated power							
FCS-3	0.6	20	45.5	52.3	48.3	2.4	−1.4
Effect of removing expander							
FCS-2	0.7	5	41.6	50.4	45.1	2.3	−7.9
Effect of maximum turndown of CEM							
FCS-1	0.7	15	45.7	53.0	48.7	2.5	−0.6
FCS-1	0.7	7	44.2	52.1	47.4	2.4	−3.2
FCS-1	0.7	3	40.6	49.8	44.3	2.2	−9.7
FCS-1	0.7	2.5	38.6	48.4	42.5	2.1	−13.3

relation of fuel cell stack data. We also examined the influence of a more aggressive polarization curve (i.e., a higher-performing fuel cell) derived from recent laboratory data on small test cells (see Fig. 3). In the more aggressive polarization curve, the cell voltage at a given current density is less sensitive to system pressure. Table 4 indicates that the fuel economy multiplier for the SUV platform improves by about 6% with the more aggressive polarization curve.

We have also analyzed the effect of selecting a design point cell voltage of 0.6 V (FCS-3) rather than the 0.7 V (FCS-1) used in the base case. At the lower cell voltage, the cell-level power density (in terms of W/cm^2) is almost 40% higher than at 0.7 V per cell. This makes for a smaller, less expensive stack because of the decreased fuel cell active area, but lowers the design point system efficiency. The results are summarized in Table 4, which shows that use of FCS-3 instead of FCS-1 in the SUV platform results in less than 2% decrease in the fuel economy multiplier. Even though FCS-3 is almost 15% less efficient than FCS-1 at the rated power point, the system efficiency is only slightly lower at partial loads. The vehicles' fuel economy is determined over the FUDS and FHDS, however, which do not require the full rated power at any time during the driving schedules. As shown earlier in Table 1, the difference in efficiencies of FCS-1 and FCS-3 is less than 2% (61.6% versus 60.1%) at 25% of rated power. Consequently, the fuel economy multiplier for the H_2-FCV versus the ICEV decreases very little if the design point cell voltage is 0.6 rather 0.7 V.

The power consumed by CEM represents the largest parasitic loss in the fuel cell system. The fuel economy multiplier can be degraded if the compressor is not as efficient at part load as implied in Fig. 2, does not have the expander, does not have the necessary turndown, or operates as a positive displacement device and delivers air at constant or high pressure at part load.

We have evaluated the change in fuel economy with removal of the expander, i.e., by using FCS-2 rather than FCS-1 as the fuel cell system configuration for the SUV. Table 4 shows that the effect of removing the expander is to decrease the fuel economy multiplier by about by about 4% even though FCS-2 is almost 7% less efficient than FCS-1 at the rated power point.

We have also analyzed how the fuel economy of the H_2-FCVs is affected by the maximum turndown of the CEM by varying the minimum "idling" air flow rate and CEM power consumption. Table 4 shows that the fuel economy multiplier decreases by less than 1% if the maximum turndown is 15 rather than the theoretically available value of 20, by about 3% if the maximum turndown is seven, by about 10% at maximum turndown of three and by about 13% at maximum turndown of 2.5.

4.3. Effects of improved H_2-FCV parameters

We have investigated the potential for further improvements in the fuel economies of the two smaller vehicles—the Cavalier and the Taurus—by considering versions of these two vehicles with reduced mass (same as for the ICE version); lower drag coefficient, by improving the vehicles' aerodynamics; and decreased coefficients of rolling friction, by using, for example, advanced tires. The modified parameters, and the resulting fuel economies, are summarized in Table 5. These results show that significant further increases in fuel economy are possible if these vehicle improvements can be achieved.

The fuel economy multipliers listed in the last row of Table 5 are relative to the conventional ICE vehicles. Of course, with the improved vehicle parameters, the ICEVs' fuel economy would also be improved. In the present discussion, however, we are assessing the potential for improvement in vehicle fuel economy using advanced technologies as compared to current

Table 5
Increase in fuel economy of Cavalier and Taurus with improved vehicle parameters

Parameter		Cavalier		Taurus	
		H_2-FCV	H_2-FCV (improved)	H_2-FCV	H_2-FCV (improved)
Mass (kg)		1400	1214	1850	1693
Drag coefficient		0.38	0.26	0.32	0.26
Frontal area (m^2)		1.8	1.8	2.2	2.2
Coefficient of rolling friction		0.009	0.006	0.009	0.006
"Engine" power (kW)		90	90	120	120
Fuel economy (mpgge)	FUDS	73	83	58	62
	FHDS	75	101	69	84
	Combined	73.8	90.0	62.4	70.4
H_2-FCV/ICEV (mpgge)		2.7	3.3	2.7	3.0

Table 6
Parameters for compressed hydrogen storage tanks for automotive applications (specifications from quantum [9])

Parameter	Specification			
	Tank 1	Tank 2	Tank 3	Tank 4
Storage pressure (psia)	5000	10,000	5000	10,000
Amount of hydrogen stored (kg)	3	3	7	7
Tank system				
Volume (l)	145	100	320	220
Weight (kg)	45	50	90	100
Tank system				
Energy density (kWh/l)	0.69	1.00	0.73	1.06
Specific Energy (kWh/kg)	2.20	2.00	2.60	2.30

gasoline ICE technology. Thus, the potential improvements in fuel economy offered by lighter, more aerodynamic, and lower-rolling-friction gasoline ICEVs are not discussed.

4.4. Onboard hydrogen storage requirements to yield 320 mile range

A significant issue for hydrogen-fueled vehicles is the amount of hydrogen that must be stored onboard to provide the desired range between refuelings. For the US passenger car market, a minimum driving range of 320 miles is considered essential for customer acceptance. The fuel economies discussed above are useful for determining the amounts of hydrogen needed for the three vehicles. The corresponding "fuel tank" weights and volumes may be determined by using the characteristics of the specific fuel tank designs or approaches, such as compressed hydrogen, liquefied hydrogen, physical or chemical hydrides, or other hydrogen-storage matrix materials (such as various forms of carbon or complex hydrides).

Table 6 lists the characteristics of representative, current-technology compressed hydrogen storage tanks. We used the energy density (kWh/l) and specific energy (kWh/kg) of the hydrogen stored in the tanks listed in Table 6 as a guide to estimate the volume and weight of compressed H_2 tanks sized for the H_2-FCVs (Cavalier, Taurus, and Explorer), as shown in Table 7. With the improved vehicle parameters (i.e., lower mass, drag coefficient, and coefficient of rolling friction), correspondingly

Table 7
Hydrogen storage system requirements and parameters for the H_2-FC Cavalier, Taurus, and Explorer to obtain a 320 mile driving range between refuelings

	Cavalier		Taurus		Explorer	
H_2-FC/ICE (mpgge)	2.7		2.7		2.5	
Recoverable H_2 needed (kg)	4.3		5.1		6.5	
Fuel tank						
Pressure (psia)	5000	10,000	5000	10,000	5000	10,000
Volume (l)	205	150	240	165	295	200
Weight (kg)	60	75	75	80	80	95

less H_2would be needed onboard the vehicles to yield the same driving range between refuelings.

5. Conclusions

- For equal LHV energy content of the fuel, the H_2-fueled fuel cell vehicles offer potential mpgge fuel economy multipliers of 2.7, 2.7, and 2.5 for a compact, mid-size, and sport utility vehicle, respectively.
- For a non-hybrid vehicle, the potential improvement in fuel economy over standard urban and highway drive schedules degrades only slightly if the design-point cell voltage is lowered from 0.7 to 0.6 V. Thus, there is little incentive in selecting a higher cell voltage at the rated power point given that the size and cost of the fuel cell stack, likely the most expensive component in the fuel cell system, increase non-linearly with increasing cell voltage.
- The power consumed by the air management system represents the largest parasitic loss in the fuel cell system. To preserve the benefit of the enhanced efficiency of the fuel cell stack at part load, it is important to select an air management system capable of achieving a reasonable turndown and operating at reduced pressures at part load where the CEM component efficiencies are generally lower.
- The compact, mid-size, and sport utility fuel-cell vehicles analyzed in this work will need 4.3, 5.1, and 6.4 kg, respectively, of recoverable H_2 stored onboard to achieve a 320-mile driving range between refuelings (based on the combined fuel economy over the US Federal Urban and Highway Driving Schedules).
- Further gains in the vehicles' fuel economies are possible if their mass, drag coefficient, and/or the coefficient of rolling friction can be reduced.

Acknowledgements

This work was supported by the US Department of Energy's Office of Energy Efficiency and Renewable Energy, Office of Hydrogen, Fuel Cells, and Infrastructure Technologies and the Office of FreedomCAR and Vehicle Technologies.

References

[1] M.A. Weiss, J.B. Haywood, A. Schafer, V.K. Natarajan, Comparative Assessment of Fuel Cell Cars, Massachusetts Institute of Technology, Laboratory for Energy and the Environment, Publication No. LFEE 2003-001 RP, February 2003.
[2] Well-to-Wheel Energy Use and Greenhouse Gas Emissions of Advanced Fuel/Vehicle Systems—North American Analysis, vol. 2, General Motors Corporation, June 2001.
[3] H.K. Geyer, R.K. Ahluwalia, GCtool for Fuel Cell Systems Design and Analysis: User Documentation, Argonne National Laboratory Report ANL-98/8.
[4] P.B. Davis, F.W. Wagner, Air Management for Fuel Cell Systems: Assessment and New Activities, SAE Paper 2002-01, SAE World Conference, Detroit, MI, 5–8 March 2001.
[5] M.K. Gee, Fuel Cell Turbocompressor, DOE Hydrogen, Fuel Cells & Infrastructure Technologies Program 2003 Merit Review and Peer Evaluation Meeting, Berkeley, CA, 19–22 May 2003.
[6] GM/Opel Set First Fuel Cell Records with Hydrogen 1, Releases New Stack Design Details, Hydrogen & Fuel Cell Letter, ISSN-1080-8019, June 2001.
[7] Ballard Sets New Standards for Automotive Fuel Cells, News Release, http://www.ballard.com, 26 October 2001.
[8] A. Rousseau, P. Pasquier, Validation Process of a System Analysis Model: PSAT, SAE Paper 01-P183, SAE World Conference, Detroit, MI, 5–8 March 2001.
[9] N. Sirosh, DOE Hydrogen Composite Tank Program, DOE Hydrogen, Fuel Cells & Infrastructure Technologies Program 2003 Merit Review and Peer Evaluation Meeting, Berkeley, CA, 19–22 May 2003.